JUL 23 1991

AEDC-TR-90-16

C.3

Ultraviolet/Visible Spectral Radiance for the Bow Shock of a Projectile Launched at High Velocities in the AEDC Track G Facility

K. L. Dietz and W. K. McGregor
Sverdrup Technology, Inc., AEDC Group

May 1991

Final Report for Period May 1989 – June 1990

PROPERTY OF U.S. AIR FORCE
AEDC TECHNICAL LIBRARY

TECHNICAL REPORTS
FILE COPY

Approved for public release; distribution is unlimited.

ARNOLD ENGINEERING DEVELOPMENT CENTER
ARNOLD AIR FORCE BASE, TENNESSEE
AIR FORCE SYSTEMS COMMAND
UNITED STATES AIR FORCE

NOTICES

When U. S. Government drawings, specifications, or other data are used for any purpose other than a definitely related Government procurement operation, the Government thereby incurs no responsibility nor any obligation whatsoever, and the fact that the Government may have formulated, furnished, or in any way supplied the said drawings, specifications, or other data, is not to be regarded by implication or otherwise, or in any manner licensing the holder or any other person or corporation, or conveying any rights or permission to manufacture, use, or sell any patented invention that may in any way be related thereto.

Qualified users may obtain copies of this report from the Defense Technical Information Center.

References to named commercial products in this report are not to be considered in any sense as an endorsement of the product by the United States Air Force or the Government.

This report has been reviewed by the Office of Public Affairs (PA) and is releasable to the National Technical Information Service (NTIS). At NTIS, it will be available to the general public, including foreign nations.

APPROVAL STATEMENT

This report has been reviewed and approved.

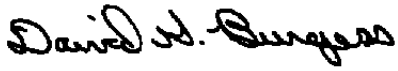

DAVID G. BURGESS, Capt, USAF
Directorate of Technology
Deputy for Operations

Approved for publication:

FOR THE COMMANDER

KEITH L. KUSHMAN
Technical Director
Directorate of Technology
Deputy for Operations

REPORT DOCUMENTATION PAGE

Form Approved
OMB No. 0704-0188

Public reporting burden for this collection of information is estimated to average 1 hour per response, including the time for reviewing instructions, searching existing data sources, gathering and maintaining the data needed, and completing and reviewing the collection of information. Send comments regarding this burden estimate or any other aspect of this collection of information, including suggestions for reducing this burden, to Washington Headquarters Services, Directorate for Information Operations and Reports, 1215 Jefferson Davis Highway, Suite 1204, Arlington, VA 22202-4302, and to the Office of Management and Budget, Paperwork Reduction Project (0704-0188), Washington, DC 20503

1. AGENCY USE ONLY (Leave blank)	2. REPORT DATE	3 REPORT TYPE AND DATES COVERED
	May 1991	Final - May 1989 - June 1990

4 TITLE AND SUBTITLE
Ultraviolet/Visible Spectral Radiance for the Bow Shock of a Projectile Launched at High Velocities in the AEDC Track G Facility

5. FUNDING NUMBERS
PN - DA93
F40600-85-C-0026

6. AUTHOR(S)
Dietz, K. L. and McGregor, W. K., Sverdrup Technology, Inc., AEDC Group

7. PERFORMING ORGANIZATION NAME(S) AND ADDRESS(ES)
Arnold Engineering Development Center/DOT
Air Force Systems Command
Arnold Air Force Base, TN 37389-5000

8. PERFORMING ORGANIZATION REPORT NUMBER
AEDC-TR-90-16

9. SPONSORING/MONITORING AGENCY NAMES(S) AND ADDRESS(ES)
Arnold Engineering Development Center/DO
Air Force Systems Command
Arnold Air Force Base, TN 37389-5000

10. SPONSORING/MONITORING AGENCY REPORT NUMBER

11. SUPPLEMENTARY NOTES
Available in Defense Technical Information Center (DTIC).

12a DISTRIBUTION/AVAILABILITY STATEMENT
Approved for public release; distribution is unlimited.

12b. DISTRIBUTION CODE

13. ABSTRACT (Maximum 200 words)

An optical arrangement and detector gating scheme for viewing the bow shock spectral radiation from projectiles launched in a hypervelocity ballistic range are reported. Velocities were about 18,000 fps. Range pressure was 49 torr of dried air. A 0.32-m grating spectrometer with a linear array optical detector was used. Gating times of 275 and 100 μsec were employed to view nose cap radiation during the projectile's flight.

The spectrum was dominated by a strong continuum in the visible with molecular band structure superimposed on it. The most dominant radiators in the UV were identified as the NO γ bands and OH. N_2^+ First Negative, N_2 Second Positive, CN, and NH were identified as emitters in the near-UV and VIS. In addition, there were many unidentified radiators in the VIS.

14. SUBJECT TERMS	15. NUMBER OF PAGES
ultraviolet spectroscopy, visible spectroscopy, bow shock, air radiation, shock cap	32
	16. PRICE CODE

17. SECURITY CLASSIFICATION OF REPORT	18 SECURITY CLASSIFICATION OF THIS PAGE	19. SECURITY CLASSIFICATION OF ABSTRACT	20. LIMITATION OF ABSTRACT
UNCLASSIFIED	UNCLASSIFIED	UNCLASSIFIED	SAME AS REPORT

PREFACE

The work reported herein was conducted by the Arnold Engineering Development Center (AEDC), Air Force Systems Command (AFSC), under Program Element Number 921F01, with sponsorship of the U. S. Army Strategic Defense Command (SDC). The work was performed in the von Kármán Gas Dynamics Facility (VKF) during May 1989. The tests were conducted by Calspan Corporation/AEDC Operations; the data discussed in this report were obtained by Sverdrup Technology, Inc., AEDC Group (a Sverdrup Corporation Company) and Calspan Corporation, operating contractors at AEDC, Arnold Air Force Base, Tennessee. The AEDC Project Number for the test phase was CJ73VG. The Air Force Project Manager for this phase was Mr. Pat Lampton. The AEDC Project Number for the data analysis/reporting phase was DA93EW. The Air Force Project Manager for this phase was Capt. Dave Burgess. The data analysis was completed June 1, 1990, and the manuscript was submitted for publication on August 15, 1990.

Acknowledgement is given to Dr. Chad Limbaugh for his assistance in interpreting the data and to Ms. Keely Beale, who operated the spectrometer. Acknowledgement is also given to Calspan Corporation personnel Mr. Tony L. Buchanan, project manager, and Mr. Howard Harris, who operated the UV and near-IR radiometers.

CONTENTS

ILLUSTRATIONS

TABLES

1.0 INTRODUCTION

The objective of the test detailed in this report was to acquire radiation and plasma/microwave interaction measurements of the bow shock formed in front of the nose cap of a hypersonic projectile. The program consisted of five shots in the AEDC Ballistic Range G. Measurements were from infrared (IR), visible (VIS), and ultraviolet (UV) radiometers, a UV/VIS spectrometer, microwave radar, laser photography, and X-ray shadowgraphs. This report is concerned only with the UV/VIS spectrometer results acquired on the first two of the five shots. The results have been presented in Ref. 1.

A fast gated (electronically shuttered) UV/VIS spectrometer was used to acquire UV/VIS spectra of the bow shock on two projectiles with velocities of 18,000 fps. Data were acquired in support of the Strategic Defense Initiative Organization (SDIO) Bow Shock Ultraviolet Experiment, an experiment based on the theory that a missile moving through the upper atmosphere during its boost phase will produce a UV signal that can be detected by a space-based sensor.

2.0 BACKGROUND

During the late 1950's and 1960's several investigations were performed with shock tubes to aid in the prediction of radiative heating of hypervelocity reentry vehicles (Refs. 2–4). From these investigations and from current shock tube investigations in support of the SDIO program (Ref. 5) it was expected that the ultraviolet region would be dominated by emissions from the NO gamma bands, N_2, O_2 and there would be a continuum throughout the visible region. Reference 6 presents the spectral radiation measurements of the leeside shock layer and wake of the space shuttle during the high-altitude portion of reentry. Identified emitters were N_2 First and Second Positive systems, the N_2^+ First Negative system, and the sodium D-lines. The continuum is most likely attributable to radiative recombination of free electrons and ions or from bremsstrahlung radiation.

Emissions from CN and NH were reported by other authors and labeled as common contaminants in shock tubes. Sodium is another common contaminant, but it was not seen in the present spectra.

3.0 APPARATUS

3.1 TRACK G FACILITY AND PROJECTILE

The tests were conducted in the AEDC VKF Hypervelocity Range/Track G, illustrated in Fig. 1. The facility's three main components are the launcher, the 880-ft track assembly contained within a 10-ft-diam tank, and the 500-ft recovery tube.

The launcher is a 150-ft-long, two-stage 2.5-in.-caliber gun. In the gun a powder is ignited to drive a piston that compresses a column of hydrogen gas. The compressed gas accelerates the projectiles to velocities just over 18,000 fps (5.5 km/sec). The expanding gas is absorbed into the volume of the blast chamber. At the front end of the blast chamber the projectile is matched to the 880-ft four-point track, as illustrated in Fig. 2. The tank was evacuated to 49 torr of dried air that had been dried to $-5°F$ dewpoint (970 ppm of H_2O), but it is believed that a small amount of additional water vapor outgassed from the walls of the chamber. Knowing the existence of a small amount of water vapor in the chamber is important in the identification of OH in the measured UV spectra.

The projectile illustrated in Fig. 3 was a polished aluminum nose tip with a 1.25-in. radius mounted in a 2.5-in.-diam cylindrical Lexan® base. The model was 3.9 in. long. Indicated on the figure are the estimated conditions behind the shock: 840 atm pressure and 16,000 K.

The shock standoff distance was determined from laser photographs. Two independent laser cameras were aimed into the track at different positions downrange. The cameras imaged the standoff distance at the nose tip and at other points along the projectile body as the model moved down the track. For Shot 6505, the two measured shock standoff distances were 0.1 and 0.096 in. Elsewhere around the body the standoff distance varied from 0.091 in. to 0.13 in. For Shot 6506, the two measured shock standoff distances were 0.129 in. and 0.121 in. Elsewhere around the body the standoff distance varied from 0.116 in. to 0.143 in.

Table 1 is a summary of the facility conditions during Shots 6505 and 6506 serviced with a spectrometer, the other three shots of the test matrix, plus three shots (6412, 6413, and 6414) from an earlier test matrix with conditions similar to those for Shots 6505 and 6506. The three shots in the earlier test matrix had lower range pressures. UV and VIS radiometric measurements acquired during Shots 6412 – 6414 will be compared to the spectral data in Section 5.0.

3.2 SPECTROMETER

3.2.1 Requirements

Test requirements specified the design of a calibrated instrument that would measure a broadband UV/VIS radiance spectrum from just the bow shock. The side body of the projectile was to be avoided, as was the wake following the projectile.

Because of the projectile's small size, the system was designed with a small field-of-view (FOV) that remained completely within the boundaries of the nose cap. Because of the high

velocity of the projectile, the complete spectrum was acquired in a very short time, on the order of 100 μsec.

3.2.2 Hardware

The spectrometer was a 0.32-m Czerny-Turner configuration with a 147-groove/mm plane grating. The grating was blazed for 250 nm, but it had excellent response through the VIS region. Dispersion was 20.4 nm/mm in the focal plane. A UV-enhanced 1,024-element silicon diode linear array detector was used. The elements were on 0.025-mm centers. Spectral coverage was 220 to 770 nm. Spectral resolution was 2.5 nm at full-width-half-maximum (FWHM).

The entrance slit of the spectrometer was 0.025 mm wide by 1 mm high. A 6.5-in. focal length fused silica lens was used to define a rectangular FOV focused at 10 ft. At 10 ft the VIS FOV was 0.02 in. wide by 0.73 in. high. By using a folding, front-surfaced aluminum mirror the FOV was aimed diagonally across the track. A shallow angle was chosen to give the FOV the most head-on view possible. During chamber installation, the system was back-illuminated with a collimated red laser and the red beam was used to precisely point the FOV. The FOV was aimed through the track slots. It terminated on a blackened, solid portion of the track. The red laser aided in visualizing the size of the FOV. This confirmed that the FOV remained small and was completely contained within the boundaries of a 2-in.-diam circle at least 40 in. in front of and behind the focus point. This confirmed that the FOV would not grow beyond the nose cap boundaries as the projectile moved through the focus point. The placement of the FOV was also confirmed by viewing the UV and VIS emission lines of a mercury arc lamp as the lamp was scanned spatially in the track volume. A pinhole aperture was mounted on the lamp to approximate a point source.

Figure 4 is a schematic of the spectrometer as it was mounted in the hypervelocity range. The port window was fused silica with excellent UV through near-IR transmission. Figure 5 illustrates the placement of the FOV relative to the path of the projectile and the triggering events.

The detector was an EG&G Princeton Applied Research (PAR) Model 1421-B intensified UV-enhanced silicon diode array. Even though light continually entered the spectrometer, the detector was only responsive to light when a 200-v current was applied across the intensifier component. This was used to fast gate the system. As illustrated in Fig. 4, the 200-v pulse was applied to the detector by the PAR Model 1304 fast gate pulser. The Model 1304 was controlled by the computer-based PAR Model 1460 data buffer and controller.

Triggering was initiated when the model broke a laser beam 51 in. uprange from the beginning of the diagonal FOV. A time delay was programmed so that data acquisition began

after the FOV was well into the nose cap, thus avoiding detecting radiance levels from the edge of the projectile. The integration time (gate time) was programmed to end before the FOV scanned to the opposite edge of the nose cap. As the model moved down the range, the rectangular FOV was scanned across the face of the nose cap as illustrated in Fig. 6. Except for a background scan acquired 20 sec before launch, only one spectrum was acquired for each launch. After the integration time elapsed, a 5-v TTL signal was sent to the facility computer to confirm that data had been acquired.

3.2.3 Calibration and Data Reduction

The spectrometer was calibrated for wavelength against the known UV and VIS emission lines of a mercury/argon lamp. Table 2 lists the element location of the known emission lines. By performing a least-squares operation with the measured element-line pairs, coefficients A_0 through A_3 were calculated such that a wavelength value was assigned to each element by the equation

$$W(i) = A_0 + A_1 \cdot i + A_2 \cdot i^2 + A_3 \cdot i^3 \quad (1)$$

where i indicates the ith element. The A_2 and A_3 coefficients are small corrections to a nearly linear function. Individual narrow emission lines bloomed into neighboring elements. Typical FWHM measurements were 5 elements, or 2.5 nm. This was the spectral resolution. The wavelength calibration is known within the order of the resolution, ± 2.5 nm.

The spectrometer was calibrated for spectral radiance against a 1,000-w tungsten-halogen irradiance standard illuminating a calibrated Lambertian reflection screen. By knowing the spectral power output of the lamp standard and the spectral reflection of the Lambertian screen, researchers can use the Lambertian screen and lamp combination as a radiance standard. The calibration procedure was to focus the system into the radiance standard and acquire a background-corrected spectrum. This spectrum was divided by the known spectral radiance function of the lamp and screen. Calibration was conducted with the port window and mirror included in the optical axis as they were used during the test.

A concern of the calibration was that it was not possible to acquire a spectrum of the radiance standard in the fast gate mode because the signal was too weak. The detector has two modes of operation, a continuous mode and a fast gate mode. The fundamental difference between the modes is that in the continuous mode the high voltage is continuously applied to the intensifier component and in the fast gate mode the voltage is applied for a very short time. The detector has a response rise time on the order of a few milliseconds. In the continuous mode the detector is always at its maximum response level. In the fast gate mode the detector is operated during its response rise time.

Because it was necessary to acquire the calibration data in the continuous mode, it was necessary to confirm that the system was linear with exposure time in both modes and that there was a valid conversion factor between modes.

Figure 7 presents normalized detector signal level at three wavelengths for both modes. The data on Fig. 7 are normalized to force the continuous mode signal levels to a value of 15 at a 15-msec exposure time for convenience of presentation. Both modes are linear. There is a factor of 0.54 between the modes at all exposure times. This experiment was repeated several times, with the same results within 5 percent. Thus, the use of the 0.54 factor allows direct comparison of results obtained with the two modes.

The calibration spectrum was also corrected for second-order effects by acquiring a spectrum of the radiance standard with a Schott® 450-nm longpass filter in the optical path. The filter eliminated all radiation below 420 nm so a measure of the effect of radiation below 420 nm in second order could be made on the signal above 420 nm. The second-order effect was measured as an increase in measured radiance of 2 percent. It was corrected for by subtraction from the calibration scan used to calculate the response function.

Response functions valid for 275- and 100-μsec integration times were calculated as

$$R_{275}(\lambda) = \frac{C_{15}(\lambda) \cdot 0.54 \cdot 0.275}{15 \cdot RAD(\lambda)}$$

$$R_{100}(\lambda) = \frac{C_{15}(\lambda) \cdot 0.54 \cdot 0.100}{15 \cdot RAD(\lambda)} \quad \frac{\text{counts}}{\mu w/sr \cdot cm^2 \cdot nm} \tag{2}$$

where C_{15} (λ) is the digitized count level from the detector array as the system viewed the radiance standard for 15 msec, and RAD(λ) is the known radiance function of the radiance standard. Figure 8 presents the response functions used to calculate the spectra for the two shots. Data reduction was accomplished by subtracting the background spectrum from the raw data and dividing the results by the response function. The reduced data values of the spectrum were then divided by 1,000 and presented in units of mw/sr • cm^2 • nm.

3.3 RADIOMETERS

3.3.1 UV Radiometers

Two UV radiometers were used to acquire in-band radiance measurements on two shots not serviced by the UV/VIS spectrometer (Shots 6412 and 6414). The shots were similar,

and the data are compared to the UV/VIS spectra in Section 5.0. Bandpasses were 317 to 393 nm and 349 to 492 nm. They were mounted 18.6 ft uprange of the spectrometer's position, 90 deg to track centerline. The FOVs, limited by knife edges placed on the track slots, were the same, 1.25 in. wide by 0.5 in. high.

The radiometers were calibrated against a standard quartz lamp and focused onto the calibration source. From the known radiant intensity of the standard and the measured response in volts, the response function of intensity per volt was calculated. The voltage measured during the test was then reduced by multiplication by the response function.

Data were archived in units of w/sr-μm. For this report, the values were divided by the FOV area and converted to units of mw/sr-cm^2-nm for comparison to the spectrometer data.

3.3.2 Near-IR Radiometer

The UV radiometers were replaced by one near-IR radiometer on Shots 6505 and 6506 serviced by the UV/VIS spectrometer. The near-IR radiometer had the same FOV as the UV radiometers. The bandpass was 755 - 845 nm.

Calibration and data reduction was similar to that of the UV radiometers, except the standard source was a blackbody, and the values were also divided by the axial length of the FOV.

Data were archived in units of w/sr-cm-μm where cm refers to the axial length of the FOV. For this report, the values were divided by the height of the FOV and converted to units of mw/sr-cm^2-nm for comparison to the spectrometer data.

4.0 RESULTS

UV/VIS radiance spectra were measured from the bow shock of projectiles in two launches. Chamber pressure for Shot 6505 was 49 torr (18.9-km simulated altitude). The model velocity was 18,320 fps, and the spectrometer was gated for 275 μsec. During the gate time the model flight distance was 59.8 in. in the FOV, and 1.27 in. of the nose cap was scanned by the FOV. Chamber pressure for Shot 6506 was 49 torr. The model velocity was 18,183 fps, and the spectrometer was gated for 100 μsec. During the gate time the model flight distance was 21.6 in. in the FOV, and 0.46 in. of the nose cap was scanned by the FOV.

The spectral features are a strong continuum radiation and a rich, superimposed molecular band structure. In the ultraviolet, the dominant molecular radiators are NO gamma bands which stand out clearly and are repeatable in the two spectra. OH is clearly identified as

an emitter at 281 and 310 nm. OH arises from the small amount of water vapor in the chamber. Unidentified radiators are probably NO (β and δ systems), O_2, O_2^+, N_2, or N_2^+. CN and NH, listed as common contaminants in shock tube measurements by other authors, are probable emitters.

Figure 9 presents the raw, background-corrected spectrum from both shots. Figure 10 presents the reduced radiance spectra of the two shots in the ultraviolet and visible/near-IR spectral regions.

Table 3 lists the wavelength of the emission lines of Shot 6506 and the wavelength of the most probable emitter. Emitters were identified from wavelength tables in Refs. 7 and 8. The wavelengths listed in the first column are the approximate values as a result of the system wavelength calibration.

5.0 DISCUSSION

The strong continuum in the visible is most likely attributable to electron-electron continuum and electron-ion recombination. The estimated stagnation temperature in front of the nose cap is 16,000 K at about Mach 16 conditions. At these conditions, the electron density is about 10^{15} per cm^3 (Ref. 9). The estimated pressure behind the shock is 840 atm. At this extreme pressure level the radiance would approach that of a blackbody at 16,000 K.

There is some question about the strong increase in signal with decreasing wavelength in Fig. 10a. It is similar to a blackbody function for extremely high temperatures. Figure 11 presents the blackbody function for 16,000 K. It is reasonable to conclude that the measured UV radiance is from a blackbody emission of the plasma in the shock layer just as for the VIS. But from experience in applying the spectrometer, it is known that extreme visible components of radiation entering the spectrometer are internally scattered from the inside walls and affect the UV signature. An attempt was made to correct for this scattered radiation, but a complete correction was impossible without a more extensive data set. It was impossible to determine the source of the strong apparent UV signal.

It is certain the continuum did not arise from viewing a hot aluminum nose cap surface of the projectile. If the projectile had reached high temperatures there would have been severe ablation. It was determined from laser photographs of the projectile acquired during flight that there was little to no damage to the aluminum nose cap.

Because of the possible internal scatter of radiation into the UV region, the uncertainty of the measured ultraviolet radiance is unknown, but in the VIS/near-IR region it is on the order of ±25 percent.

Table 4 presents the average visible radiances measured by the spectrometer in the 320- to 400-nm and 400- to 650-nm bands by the near-IR radiometers on Shots 6505 and 6506, and those measured by the UV radiometers on Shots 6412, 6413, and 6414. The spectrometer was not used during Shots 6412, 6413, and 6414.

The agreement, in general, is good. The 320- to 400-nm and 349- to 492-nm integrated spectrometer values are on the order of two to eight times higher than those measured by the UV radiometers, but the pressure in the chamber was higher (49 torr compared to 12 and 24 torr). Radiance would be expected to increase with increasing chamber pressure. The closest agreement is to Shot 6414, which was run at 24 torr.

The 400- to 650-nm spectrometer values are about 64 percent higher than those measured by the near-IR radiometer. Since the near-IR radiometer integrated over 755–845 nm and the spectrum (see Fig. 10b) indicates the radiance values begin to decrease with increasing wavelength past 680 nm, it is possible that the radiance function is not flat throughout the near-IR and the radiometer integrated over a spectral range with a lower radiance value.

6.0 SUMMARY AND RECOMMENDATIONS

An optical arrangement and detector gating scheme has been reported for viewing the bow shock spectral radiation from projectiles launched in a hypervelocity ballistic range. Velocities were about 18,000 fps. Range pressure was 49 torr of dried air (−5°F dewpoint, 970 ppm of H_2O). A 0.32-m grating spectrometer with a linear array optical detector was used. Gating times of 275 and 100 μsec were employed to view the nose cap radiation. This assured that neither the wake radiation nor the range radiation contaminated the measurement.

The spectrum was dominated by a strong continuum in the visible with molecular band structure superimposed on it. The most dominant radiators in the UV were identified as the NO gamma bands and OH. N_2^+ First Negative, N_2 Second Positive, CN, and NH were identified as emitters in the near UV and VIS, and there were many unidentified radiators in the VIS.

Comparisons to data acquired with UV bandpass radiometers on similar launches were good. Radiance values measured by the spectrometer system were about a factor of two to three higher than those of the UV radiometers, but the chamber pressure was lower during

the launches supported by the radiometers. Lower chamber pressure would result in a lower radiance signal from the shock cap.

Comparisons to data acquired with the near-IR radiometers on these two shots were also good, but 64 percent higher. The spectrum indicated that the radiometer bandpass might have included a spectral region of lower radiance resulting in a lower in-band measurement.

The limited amount of data is to be taken as preliminary. A much more extensive program is recommended. Recommendations for improvements of this system would be to increase the spectral resolution at the sacrifice of lowering the spectral band covered. Increasing the spectral resolution would allow a better identification of the radiators. Lowering the spectral band would allow the use of optical bandpass filters to minimize the degradation of the measurement caused by scattered light in the spectrometer. The use of a more complex double-pass spectrometer would also minimize scattered radiation. The complete UV/VIS band could be measured with multiple systems.

REFERENCES

1. Dietz, K. L., Beale, K. S., and McGregor, W. K. "Ultraviolet/Visible Spectral Radiation from the Nose Cap of a Projectile Launched in a Ballistic Range." AIAA-90-1552, AIAA 21st Fluid Dynamics, Plasma Dynamics and Laser Conference, Seattle, WA, June 18-20, 1990.

2. Kivel, B. "Radiation from Hot Air and its Effect on Stagnation-Point Heating." Avco-Everett Research Laboratory, Research Report 79 (1959), AFBMD-TR-59-20, ASTIA (AD 232 836). *Journal of the Aerospace Science*, Vol. 2, 96 (1961).

3. Camm, J. C., Kivel, B., Taylor, R. L., and Teare, J. D. "Absolute Intensity of Non-Equilibrium Radiation in Air and Stagnation Heating at High Temperatures." *Journal of Quantitative Spectroscopy and Radiative Transfer*, Vol. 1, No. 5, pp. 53-75 (1961).

4. Mies, F. M. "Continuum Radiation from Ionized Rare Gases in Reflected Waves." *Journal of Chemical Physics*, Vol. 37, No 5, pp. 1101-1111, September 1, 1962.

5. Wurster, W. H., Treanor, C. E., and Williams, M. J. "Kinetics of UV Production Behind Shock Waves in Air." AIAA-90-1666, AIAA 21st Fluid Dynamics, Plasma Dynamics and Laser Conference, Seattle, WA, June 18-20, 1990.

6. Blackwell, H. E., Scott, C. D., and Mende, S. B. "Spectral Measurements of the Space Shuttle Leeside Shock Layer and Wake." AIAA-86-1262, AIAA/ASME 4th Joint Thermophysics and Heat Transfer Conference, Boston, MA, June 2-4, 1986.

7. Pearse, R. W. B. and Gaydon, A. G. *The Identification of Molecular Spectra*. Third Edition, Chapman and Hall Ltd., London, 1965.

8. Allen, R. A. "Air Radiation Tables: Spectral Distribution Functions For Molecular Band Systems." NASA CR-557, August 1966.

9. Cambel, Ali B. *Plasma Physics and Magnetofluidmechanics*. McGraw-Hill Book Company, Inc., New York, 1963, p. 95.

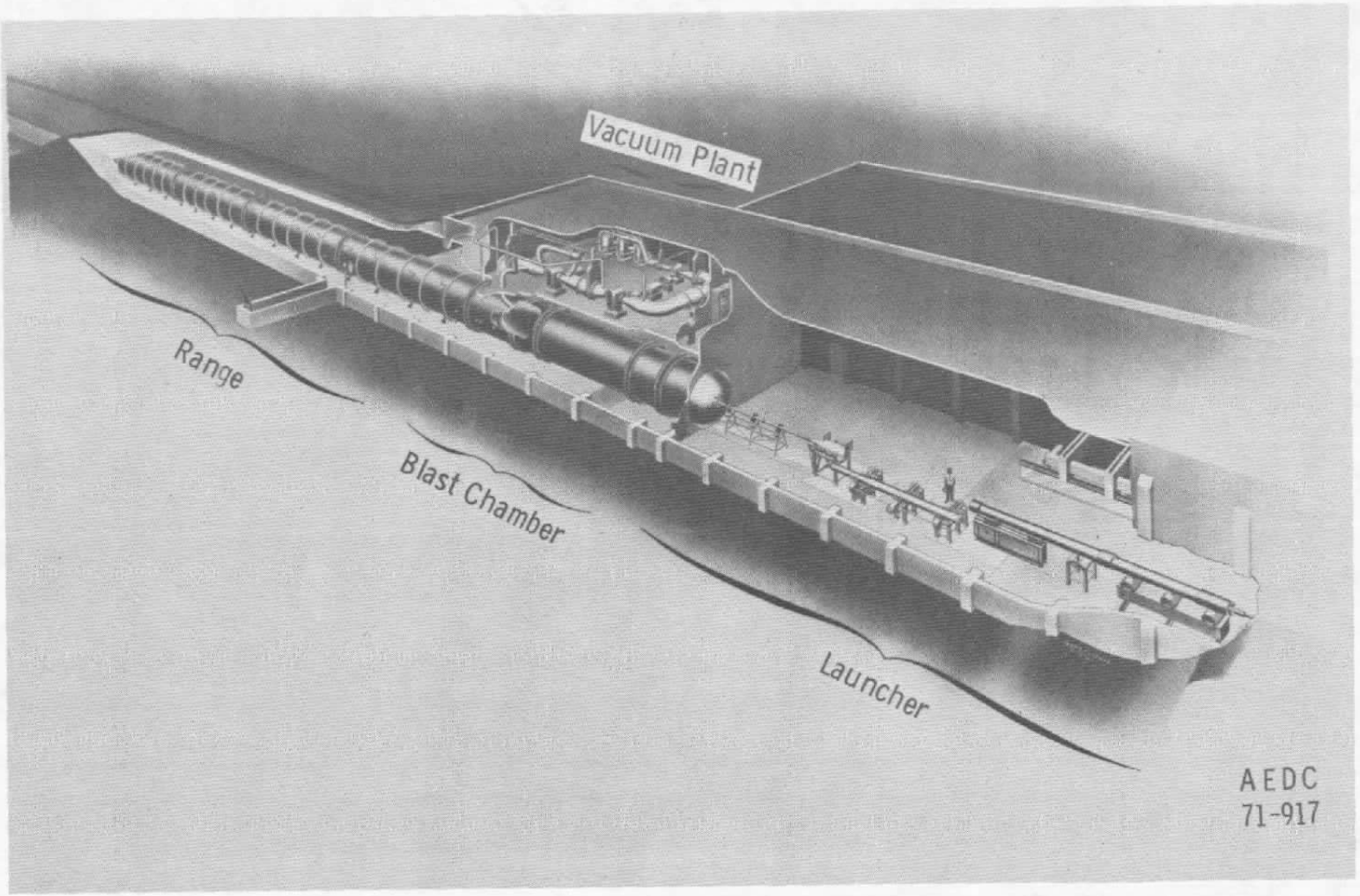

Figure 1. AEDC Hypervelocity Range/Track G.

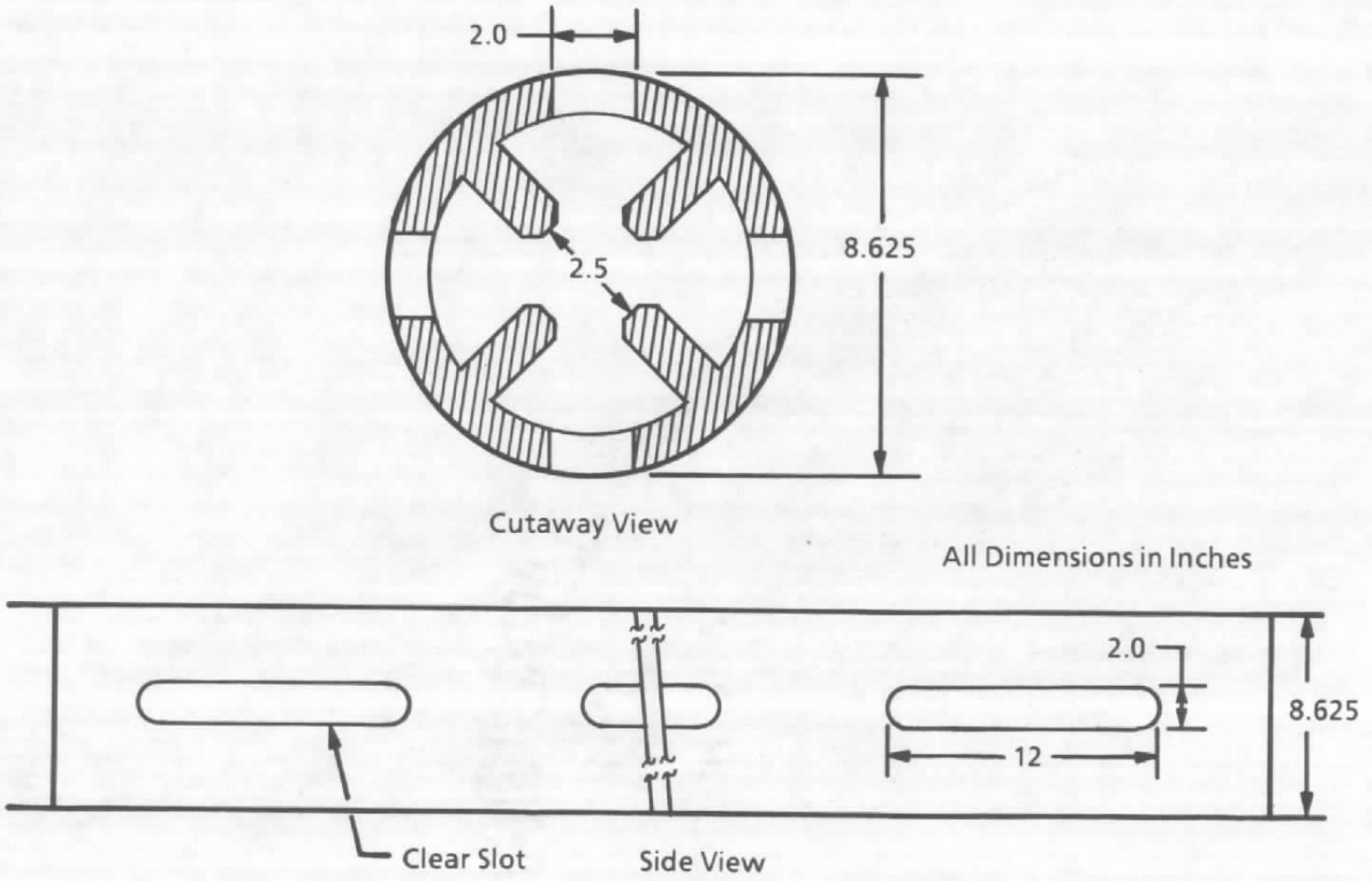

Figure 2. Typical track section.

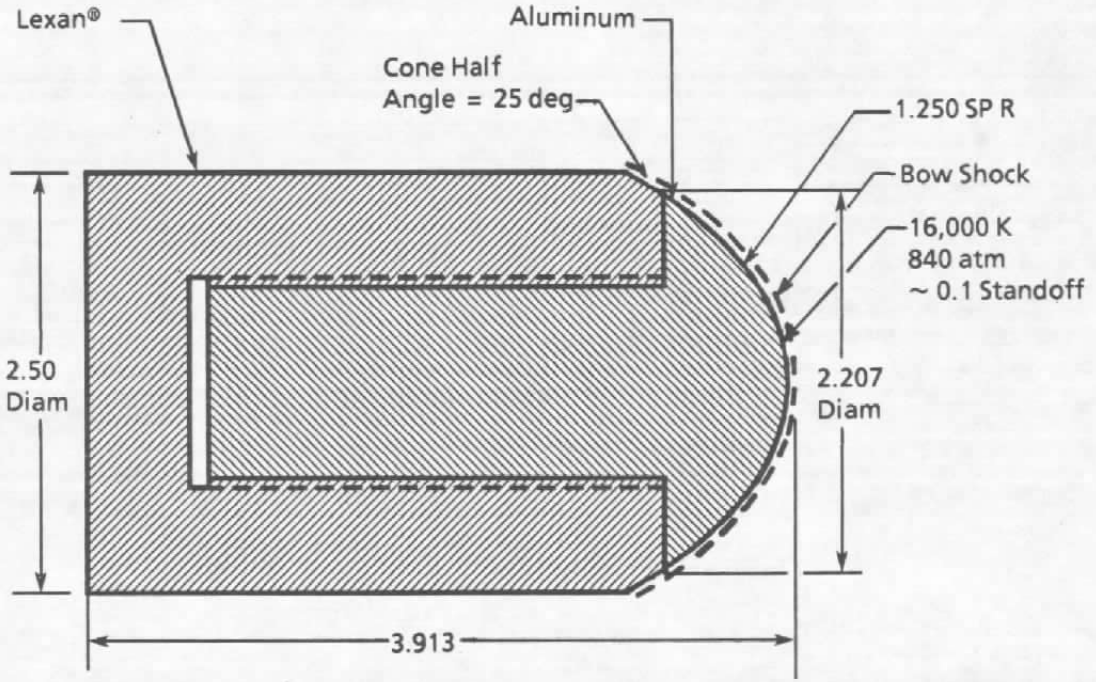

Figure 3. Illustration of projectile.

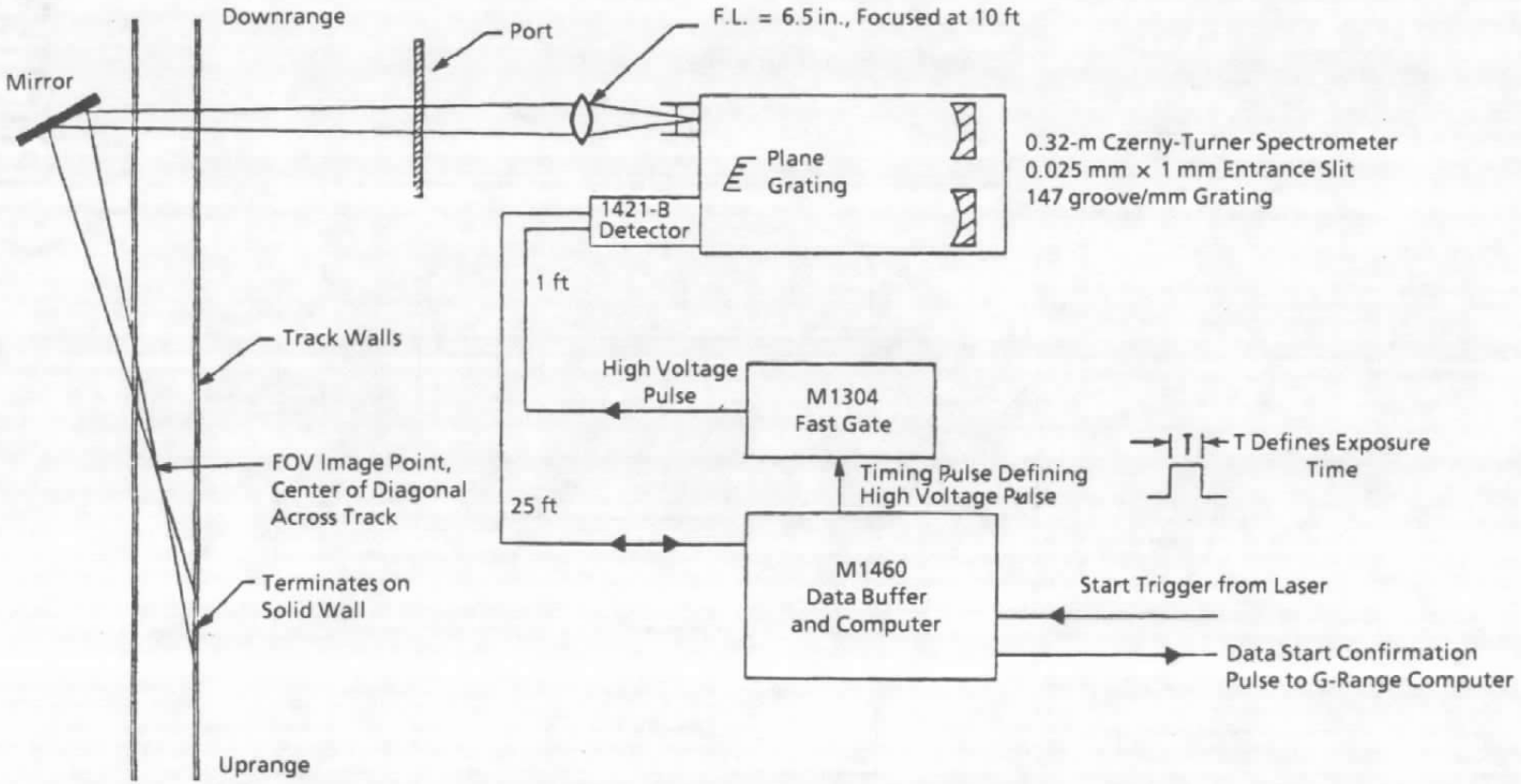

Figure 4. OMA system components as mounted in the hypersonic range.

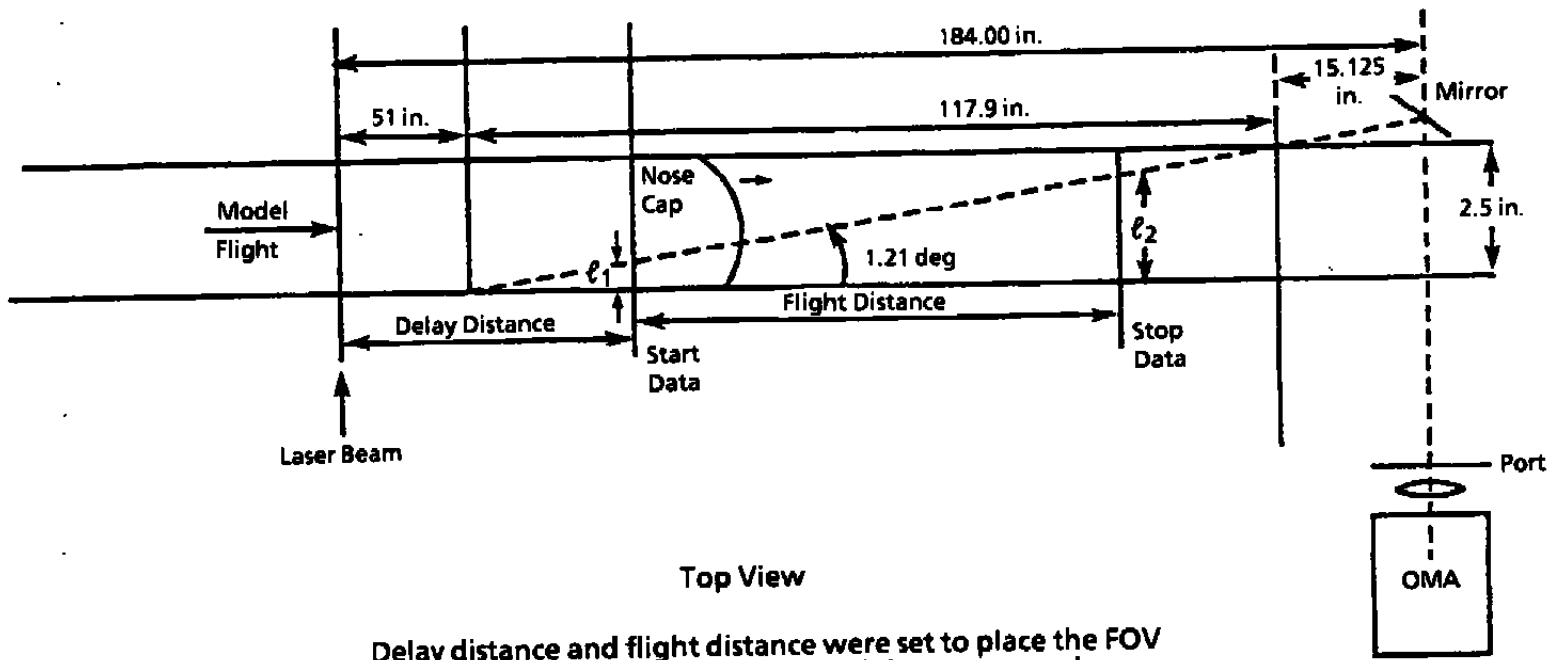

Top View

Delay distance and flight distance were set to place the FOV near the nose cap center and to avoid the nose cap edges.

Figure 5. Top view of the track and the FOV path.

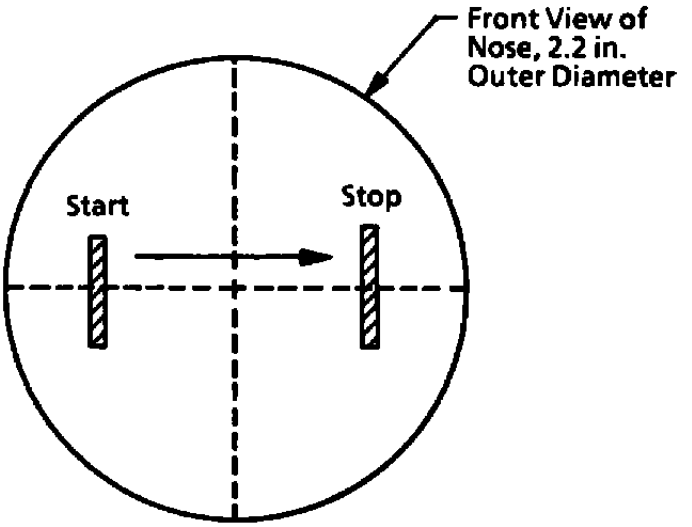

Figure 6. Illustration of the FOV scanned across the nose cap.

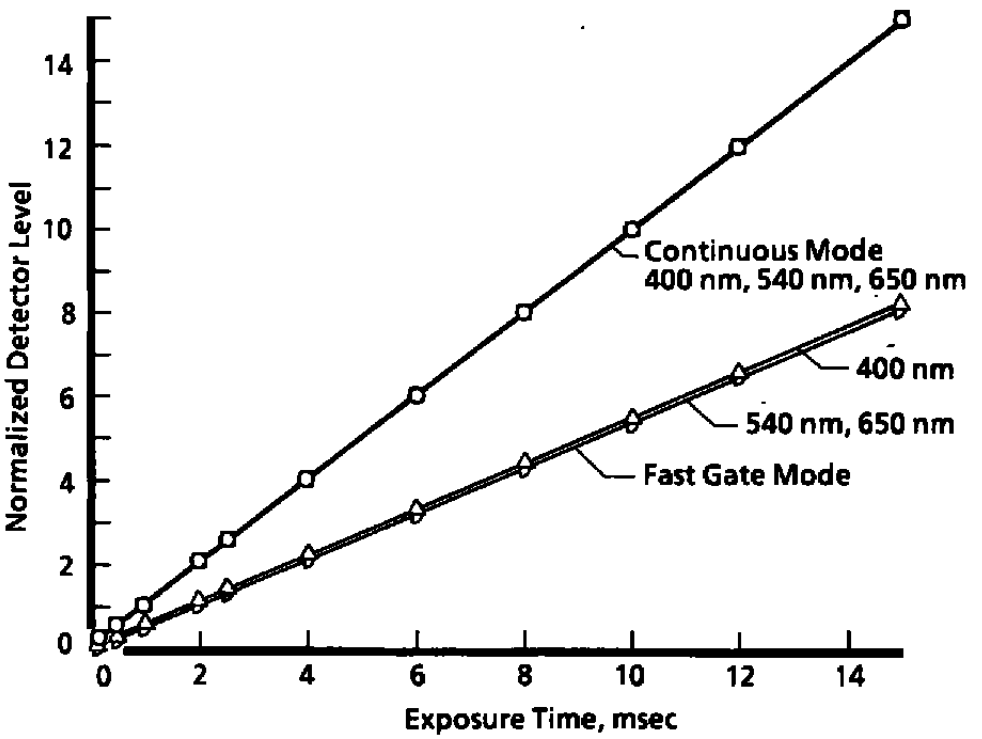

Figure 7. Normalized response to exposure time for fast gate and continuous modes.

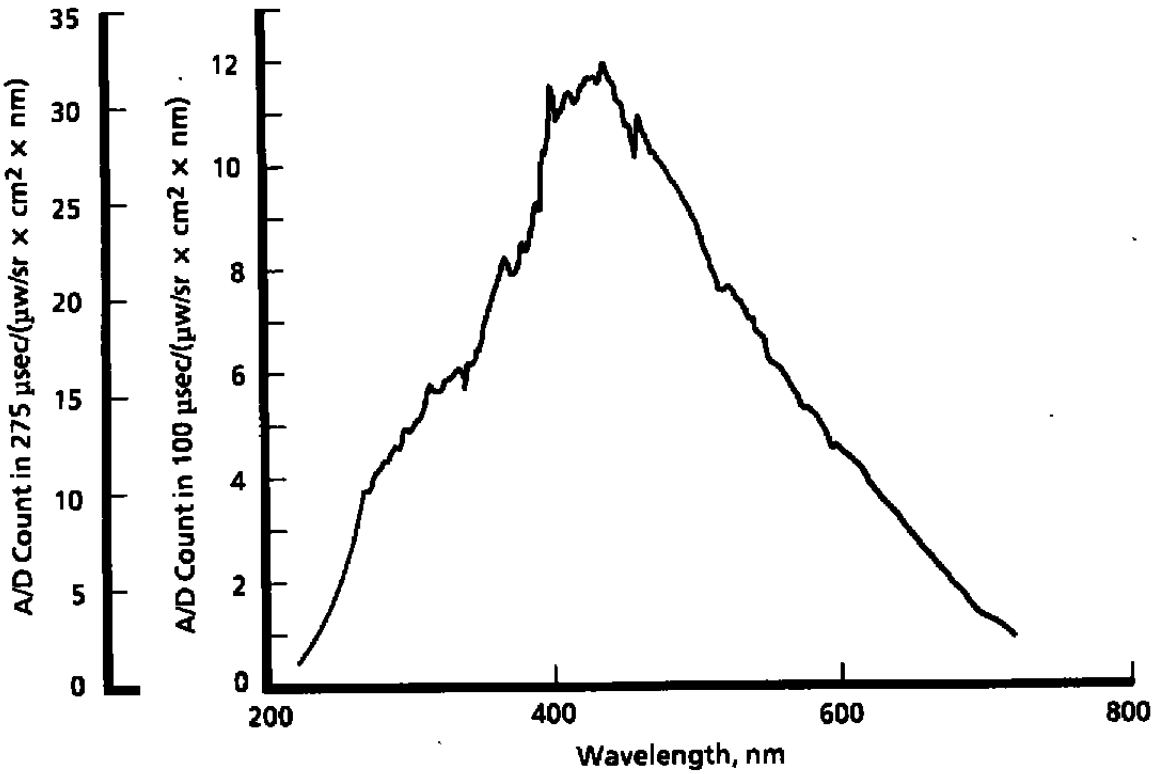

Figure 8. Spectral response function.

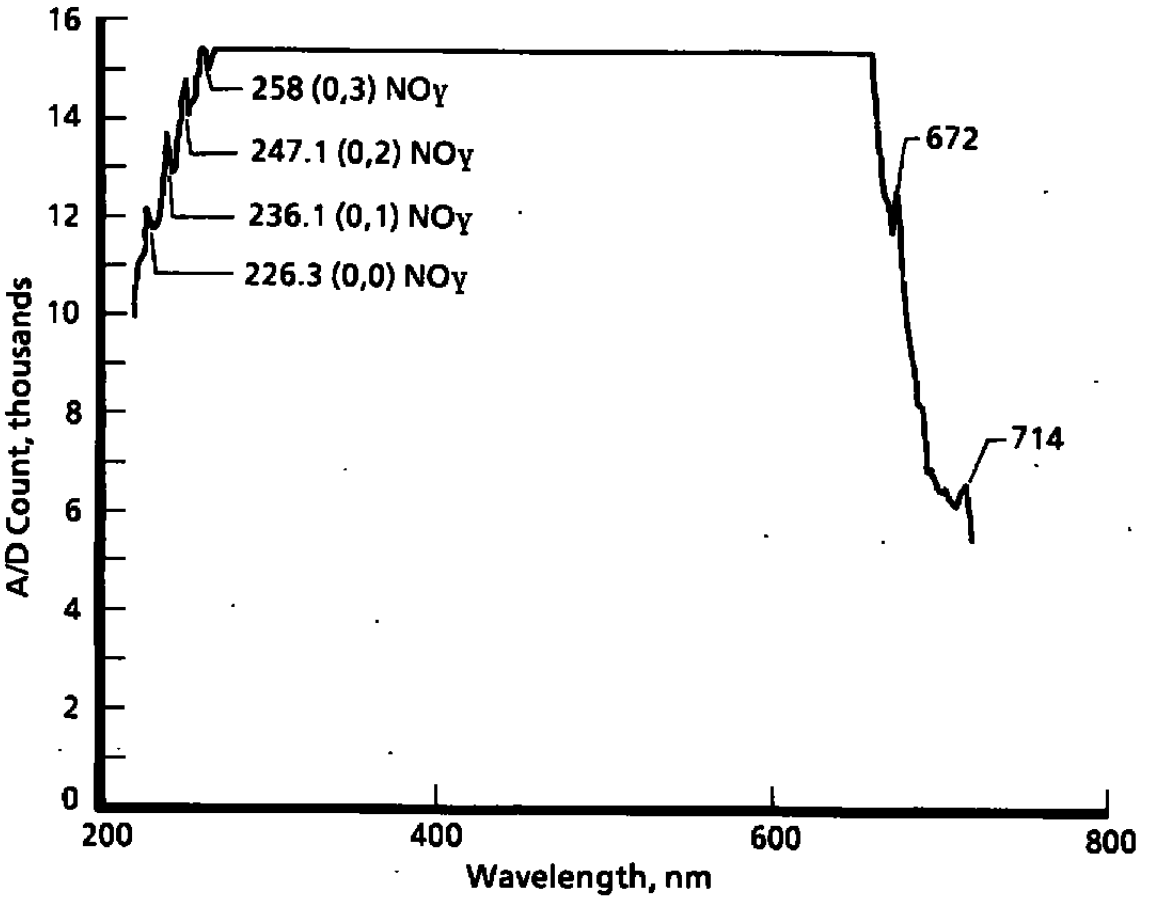

a. Shot 6505

Figure 9. Unreduced spectrum of Shots 6505 and 6506.

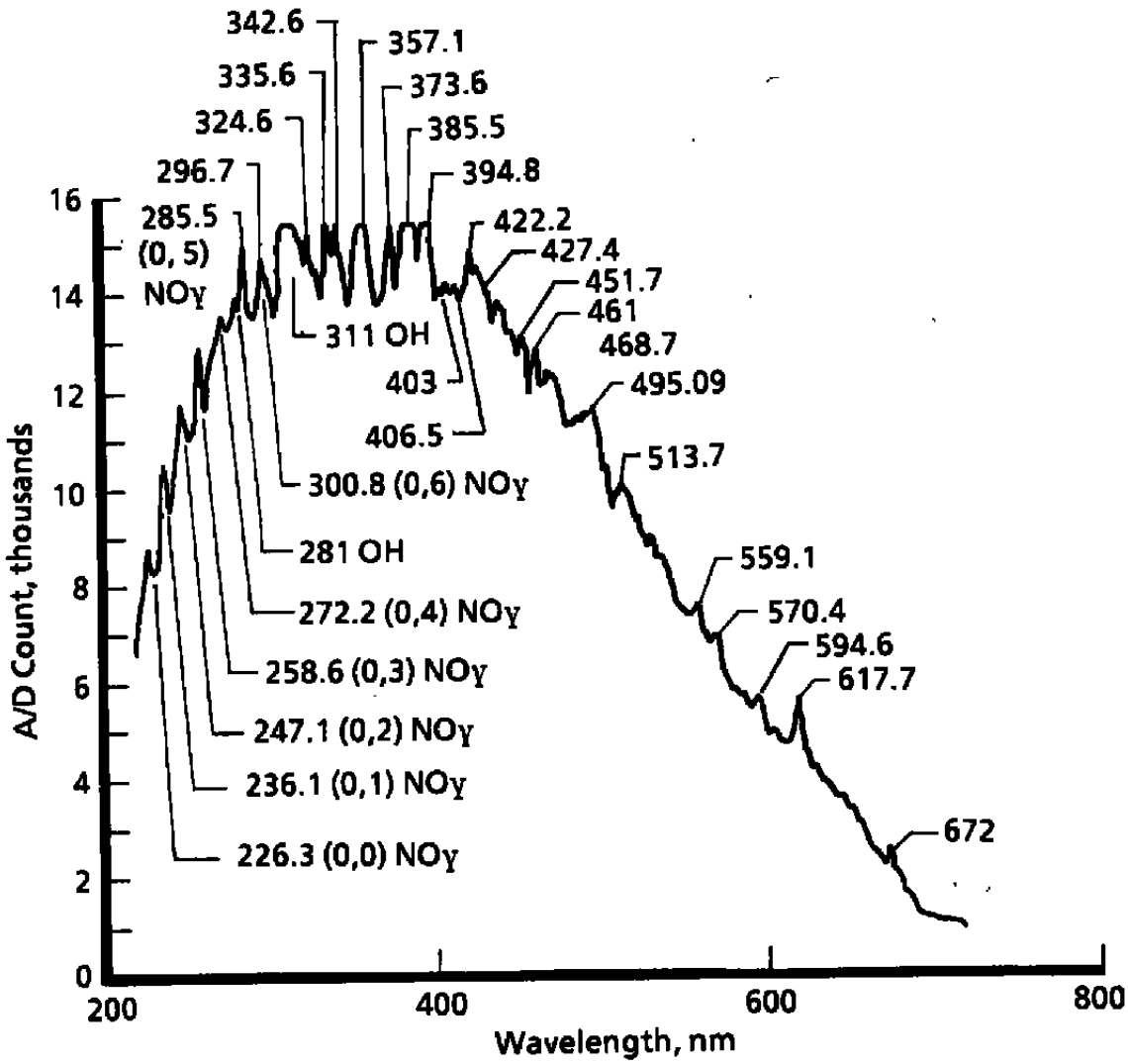

b. Shot 6506

Figure 9. Concluded.

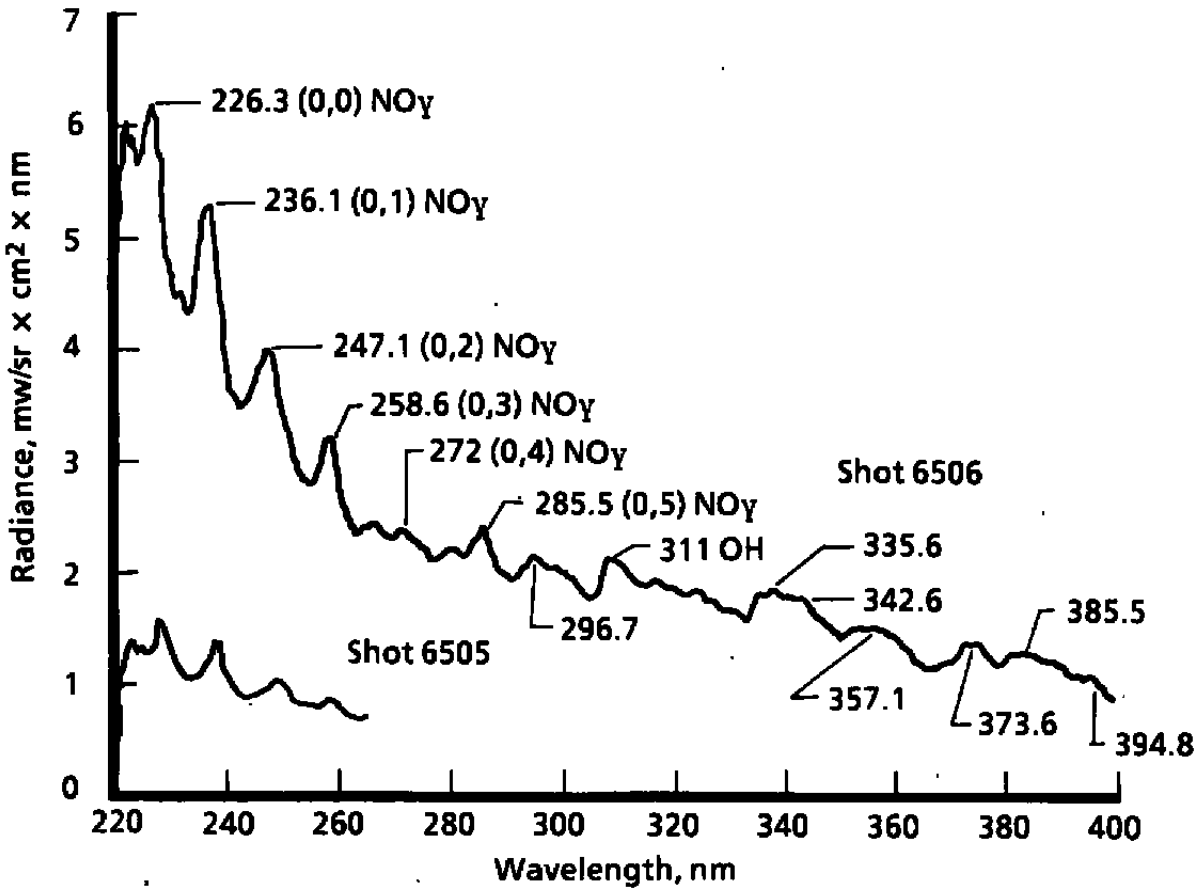

a. Ultraviolet region, 220 nm to 400 nm

Figure 10. Radiance spectra of Shots 6505 and 6506.

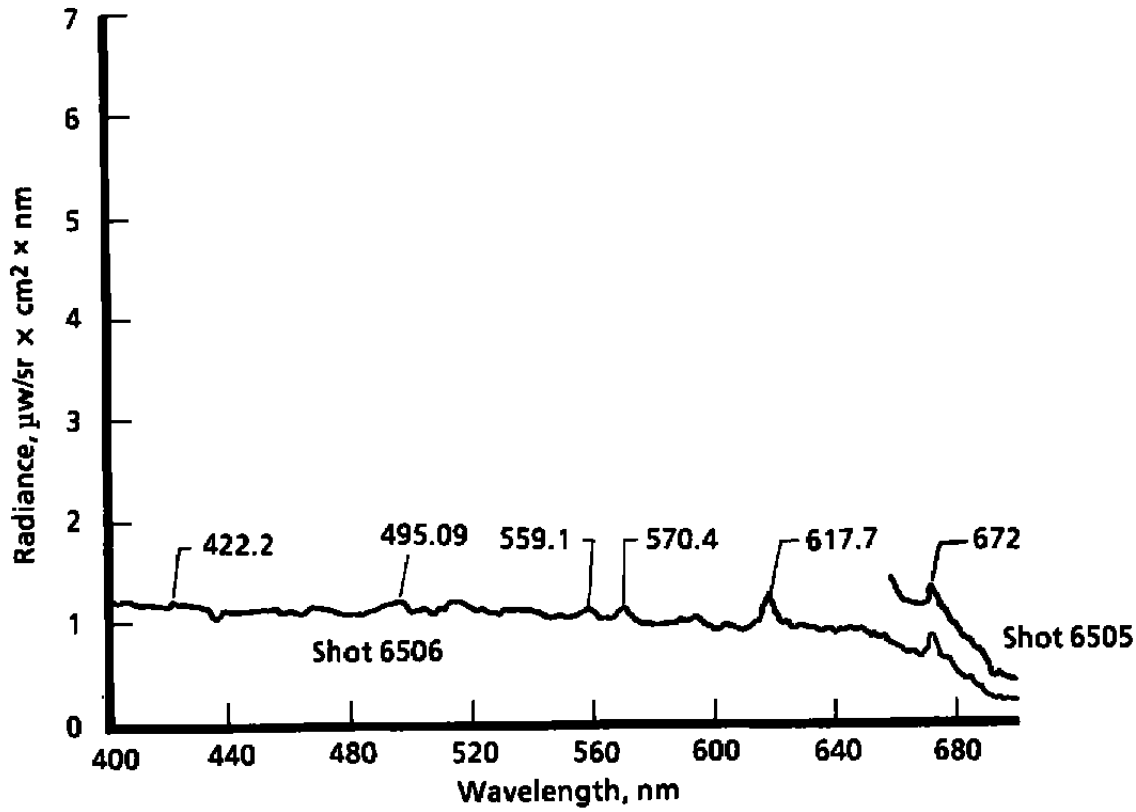

b. Visible/near-infrared region, 400 nm to 700 nm
Figure 10. Concluded.

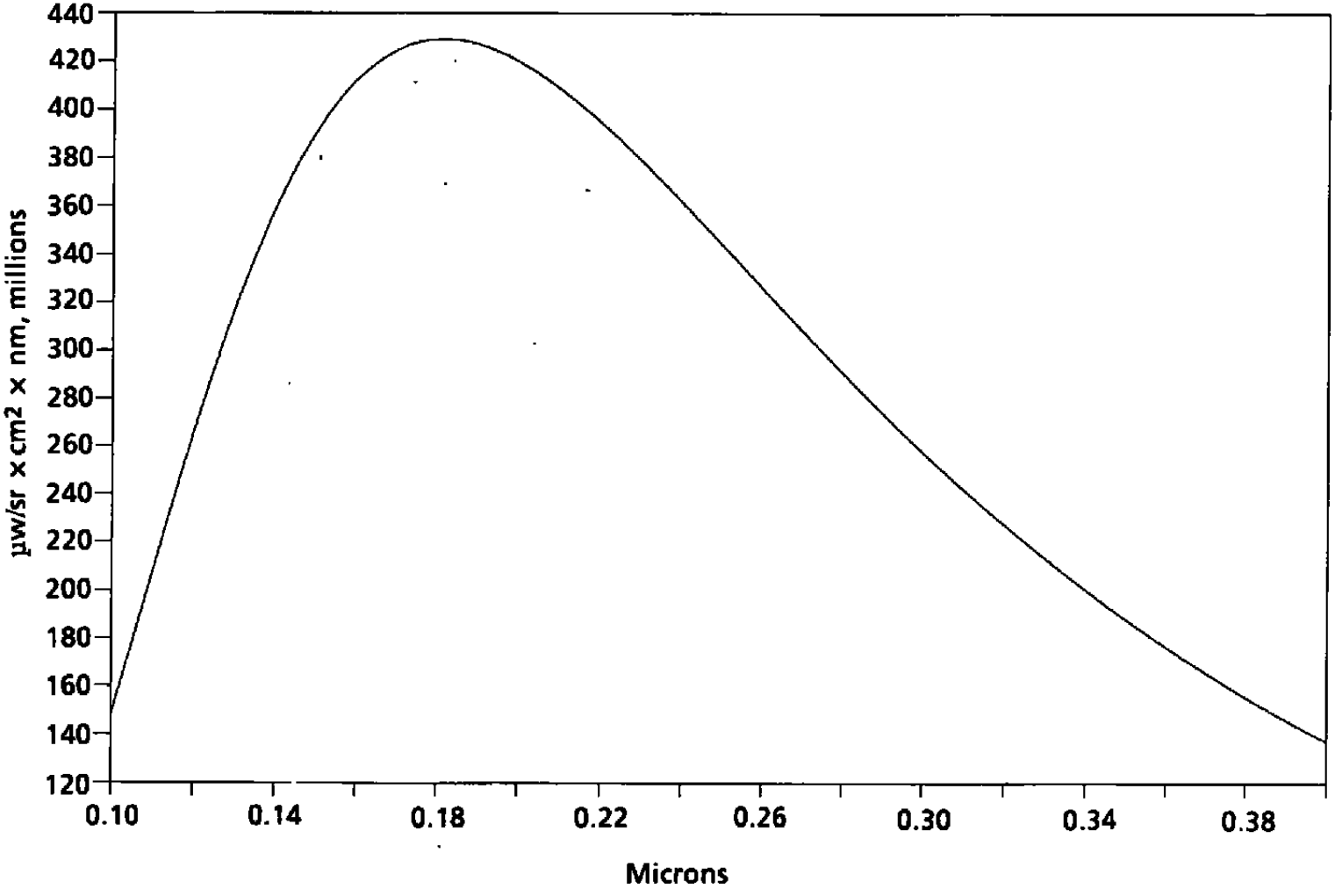

Figure 11. Blackbody radiance function for 16,000 K, ϵ = 1.

Table 1. Summary of Facility Conditions

Shot No.	Date	Velocity, fps	Dew Point, °F	Range Pressure, torr		Model Nose Radius, in.
				Blast Tank (He)	Short Range (Air)	
6505	5/13/89	18,320	−2.4	11.6	49.0	1.25
6506	5/19/89	18,183	−1.0	11.6	49.0	1.25
6507	5/22/89	18,168	−2.4	11.3	96.0	1.25
6508	5/23/89	18,484	−5.7	10.6	96.3	0.50
6509	5/24/89	16,439	—	11.3	95.9	1.25
6412	11/16/88	18,434	−23.4	10.05	12.5	1.25
6413	11/17/88	18,254	−24.7	10.00	12.2	1.25
6414	11/21/88	17,978	−21.6	10.00	24.2	1.25

Table 2. Element-Emission Line Pairs for Wavelength Calibration

Element	Emission Line, nm	Element	Emission Line, nm
122	253.7	612	507.3
204	296.7	687	546.1
236	313.1	747	577.0
336	356.0	751	579.0
412	404.7	980	696.5
473	435.87	1000	706.7

$A_0 = 192.368$ nm, $A_1 = 0.51217$ nm, $A_2 = 1.091e^{-5}$ nm, $A_3 = -8.293e^{-9}$

Table 3. Wavelength of Emission Lines in Shot 6506 Spectrum

Wavelength	Probable Emitters					
Spectrometer	NO gamma, nm	OH, nm	NH, nm	CN, nm	N_2^+ 1st Negative, nm	N_2 2nd Positive, nm
227.7	226.3 0-0					
237.0	236.1 0-1					
248.3	247.1 0-2					
258.6	258.6 0-3					
271.9	272.2 0-4					
281		281-283 1-0				
285.4	285.5 0-5					
296.7						297.68
300	300.8 0-6					
311		306-309 0-0				315.9 1-0
324.6			324.0 0-0			
Saturated 334-338			336.0 0-0 337.0 1-1	333.28	330.8 2-0	337.1 0-0
342.6						
357.1				359.04	358.1 1-0	357.7
373.6						
Saturated 381.4-389				388.3 0-0		380.5 0-2
Saturated 392.2-397					391.4 0-0	
403						
406.5						405.9 0-3
422.2				421.6 0-1		
427.4					427.8 0-1	
451.7			450.2 R 450.2 Q			
461 †				460.61		
468.7					470.9 0-2	
495.09						
513.7						
559.1						
570.4						
594.6						
617.7						
672						
714 #						

† Might not be real. Might be caused by a dip in the response function near 461 nm.
# Might be second-order 357.1 nm.

Table 4. UV and Near-Infrared Data from Spectrometer and Radiometers

Shot	Velocity fps	Pressure, torr	320-400 nm Avg. Vis Rad. from Spectrometer, mw/sr-cm^2-nm	349-492 nm Avg. Vis Rad. from Spectrometer, mw/sr-cm^2-nm	400-650 nm Avg. Vis Rad. from Spectrometer, mw/sr-cm^2-nm	0.317-0.393 Rad., mw/sr-cm^2-nm	0.349-0.492 Rad., mw/sr-cm^2-nm	0.755-0.845 Rad., mw/sr-cm^2-nm
6412	18,434	12.5				0.5	0.2	
6413	18,254	12.2				0.3	0.14	
6414	17,978	24.2				0.68	0.5	
6505	18,320	49			1.5 estimated			0.67
6506	18,183	49	1.4	1.17	1.1			0.66